Supplementary Information

Cabazitaxel-loaded redox-responsive nanocarrier of D-alpha-tocopheryl-chitosan and hyaluronic acid for improved anti-tumor efficacy in DMBA-induced breast cancer model

Abhishek Jha,[a] Manish Kumar,[a] Pooja Goswami,[b] Kanchan Bharti,[a] Manjit Manjit,[a] Ashutosh Gupta,[c] Sudheer Moorkoth,[c] Biplob Koch,[b,] Brahmeshwar Mishra.[a,*]*

[a] Department of Pharmaceutical Engineering & Technology, Indian Institute of Technology (BHU), Varanasi - 221005, Uttar Pradesh, India.

[b] Genotoxicology and Cancer Biology Laboratory, Department of Zoology Institute of Science, Banaras Hindu University, Varanasi - 221005, Uttar Pradesh, India.

[c] Department of Pharmaceutical Quality Assurance, Manipal College of Pharmaceutical Sciences, Manipal Academy of Higher Education, Manipal - 576104, Karnataka, India.

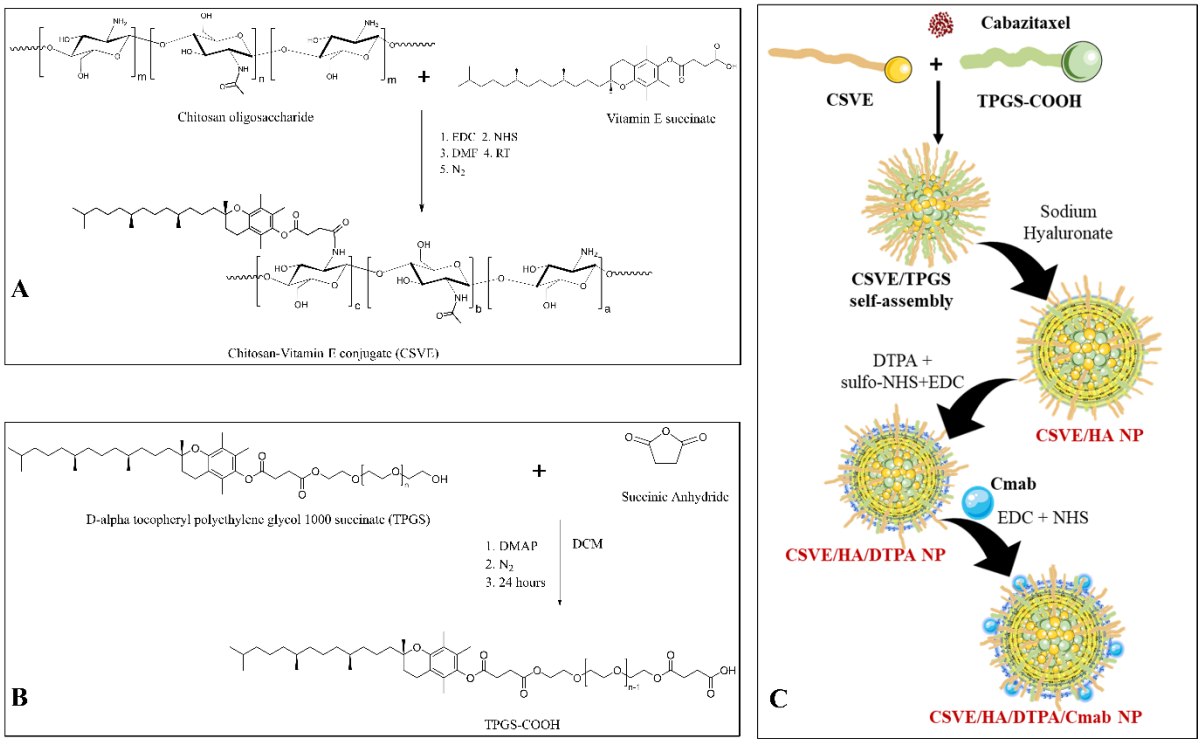

Figure S1. Schematic representation of Synthesis of CSVE (A) and TPGS-COOH (B); Preparation of CSVE/HA-based redox responsive nanoparticles (C).

Method 1: Synthesis and Characterization of TPGS-COOH and CSVE

To synthesize succinylated TPGS, 201 mg of SA and 123 mg of DMAP were dissolved in anhydrous DCM. Subsequently, 3 g of TPGS (2 mmol) was dissolved in 30 mL of anhydrous DCM and added to the above reaction mixture. The reaction mixture was purged with Nitrogen gas and maintained under a Nitrogen environment with constant stirring for the complete reaction time of 24 h at 25 °C. Then, the reaction mixture was precipitated in cold diethyl ether, and dialyzed with distilled water for 48 h using Spectra/Por® 7 dialysis membrane (MWCO; 1kDa). The purified solution was lyophilized to yield succinylated TPGS (TPGS-COOH) [1].

For synthesis of CSVE, 106 mg of VES (0.2 mmol), 383 mg of EDAC (2 mmol), and 230 mg

of NHS were added in 10 mL of anhydrous DMF under constant stirring. The reaction mixture was purged with Nitrogen gas and maintained under a Nitrogen environment. Then, 168 mg of Chitosan (equivalent to 1 mmol of glucosamine unit) dissolved in 10 mL of anhydrous DMF was added to the reaction mixture under constant stirring in the dark. The reaction continued for 24 h at 25 °C under an inert nitrogen environment. After 24 h, the reaction mixture was concentrated in a vacuum and precipitated in cold diethyl ether. The precipitation was allowed to complete overnight at -80 °C. The precipitated product was washed with ethanol three times. The washed product was consecutively dialyzed using Spectra/Por® 7 dialysis membrane (MWCO; 1kDa) against a water-ethanol mixture (1:1 v/v ratio) and distilled water for 24 h each. The dialyzed solution was then lyophilized after freezing it overnight at -80 °C to yield D-alpha-Tocopherol succinate conjugated chitosan (CSVE) [2,3].

Characterization of TPGS-COOH and CSVE was done using Fourier transform infrared (FTIR) and nuclear magnetic resonance (NMR) spectroscopy to validate the succinylation of TPGS and conjugation between VES and chitosan. FTIR spectrum of TPGS, TPGS-COOH, CSO, and CS-VE was recorded on Nicolet iS5 (Thermo Electron Scientific Instruments LLC) while their ^{1}H and ^{13}C NMR spectrum were acquired using a Bruker 500 MHz NMR Spectrometer (AVH D 500 AVANCE III HD; BRUKER BioSpin International AG). To analyze the samples by NMR spectrometer TPGS and TPGS-COOH were dissolved in deuterated Chloroform ($CDCl_3$), while CSO and CS-VE were dissolved in deuterated DMSO (d-6 DMSO).

Result 1: Synthesis of TPGS-COOH and CS-VE

The synthesis was confirmed by FTIR (**Figure. S2**) and NMR spectra (**Figure. S3**). In FTIR spectrum, characteristic peaks for TPGS were observed at 3500 cm^{-1} for terminal -OH group, 2917 cm^{-1} for alkyl -CH stretching bond of aliphatic parts of the molecule, 1742 cm^{-1} and 1646 cm^{-1} for -C=O stretching vibration, 1464 cm^{-1} for –C=C– peak of aromatic ring, 1351 cm^{-1}

for peculiar peak of $–CH_2$ group of PEG chain, 1280 and 1115 cm^{-1} for -C-O- stretching peaks. For TPGS-COOH, peaks were observed for terminal hydroxyl functional band at 3485 cm^{-1}, –CH stretching vibration of the methyl group at 2909 cm^{-1}, strong –C=O stretching vibration at 1734 with increased transmittance and peak at 1645 cm^{-1} confirmed successful synthesis of TPGS-COOH, –C=C– peak of aromatic ring at 1465, $–CH_2$ peak of PEG chain at 1353, -C-O- stretching at 1106. Chitosan exhibited characteristic peak at 3452 cm^{-1} as broad peak for hydroxyl (-OH) stretching and NH_2 group, 2925 cm^{-1} for C-H stretching, 1634 cm^{-1} for C=O stretching vibrations of N-acetylated unit of chitosan, 1520 for -NH bending, 1151 and 1073 cm^{-1} for C-O-C stretching vibrations. CSVE showed characteristic carbonyl peaks at (-C=O) at 1715 cm^{-1} and 1645 cm^{-1} (increased intensity), indicating the conjugation of acid terminal of VES to amine terminal of chitosan [2]. CSVE also showed a characteristic peak at 1566 cm^{-1} corresponding to C=O stretching vibrations of ester group of VES [4]. Reduction in free amine groups due to successful conjugation of VES and CS resulted in shielding of peak around 1520 cm^{-1} observed with CSO for NH bending. The obtained peaks indicated the successful linkage between VES and chitosan via amide bond formation.

The ^1H NMR spectra confirmed the successful synthesis of TPGS-COOH and CSVE, as shown in Fig. S3A. For TPGS, the peaks in the range of 0.8-1.0 ppm range was obtained for -CH3 protons in the aliphatic chain region, while -CH2 protons exhibited peaks in the range of 1.0-2 ppm (1). The proton peak at 1.7 correspond to -CH3 (2) while -CH3 protons attached to aromatic ring of tocopherol nucleus showed peak at 1.9-2.1 ppm (3-5). The peak for methylene proton of succinylated Vit E appears at 2.58 (6), 2.79 (7), 2.94 (9), and 4.28 ppm (8, 13). Peaks in the range of 3.6-3.8ppm (10,11) was of methylene proton of polyethylene glycol chain. For TPGS-COOH, proton peaks at approximately 2.65 ppm (14,15) belongs to the terminal succinyl methylene group [2]. Also, a peak at 3.21 ppm was observed for the methylene proton of the terminal ethylene glycol unit of PEG chain (12). Chitosan showed characteristic

anomeric proton peak at 5.31 ppm (1). The peak at 3.0 ppm was of -C2 of glucosamine (2), while protons of C3-6 is observed in the range of 3.2-3.9 ppm. The proton of C8 i.e., C2 of acetylated glucosamine unit was also observed in the same range. The 1.93 ppm peak was of the terminal methyl group (C7) of acetylated glucosamine unit. For CS-VE, the methylene proton (8,9) of succinyl group of VES and protons of -CH3 attached to the aromatic ring (10-12) was observed at 2.59 ppm and 2.51 ppm respectively. The peak in range of 0.9-1.3 ppm was for methyl proton of long aliphatic chain of VES (13) while peak at 2.85-4.03 ppm was for anomeric carbon protons of C3-6 (2-6) of CSO. The proton (7) of acetyl group attached to amine group was also observed in CSVE at 1.7 ppm. The results confirmed the successful synthesis of CSVE and were in accordance to previous reports [1].

Fig. S3B shows ^{13}C NMR spectra of TPGS, TPGS-COOH, CSO, and CSVE. The methylene and methyl carbon peaks of aliphatic chain (1) of TPGS were observed in the range of 19-25 ppm. The methyl group (3-5) attached to aromatic ring of tocopherol can be seen in the range of 11-13 ppm. The peak at approximately 27ppm denotes -CH3 carbon at position (2). The methylene carbon (6,7) of succinyl group was observed at about 32ppm. Carbon at position 8 and 9 exhibited peak in the range of 61-64 ppm. The methylene carbon of polyethylene glycol chain was seen at about 70ppm. The carbon peaks observed between 110-150 were for aromatic carbons (a-f) while peak at 170-173 belongs to carbonyl carbon (i, g) of succinyl group. In TPGS-COOH, additional two methylene carbon of succinyl group (12, 13) and two carbonyl carbons (j, k) were observed at 36-37 ppm and 170-176 ppm respectively. The spectrum of CSO showed characteristic peaks of glucosamine unit in the aliphatic region (1-6, 8, 9). Also, the carbonyl carbon (i) and methyl group of acetylated glucosamine was observed at 164 ppm and 22 ppm respectively. The spectrum of CSVE showed three carbonyl peaks (j, i, and g) in the range of 170-175 ppm, along with all the characteristic peaks of CSO and succinylated tocopherol, suggesting the successful conjugation of CSO and VES.

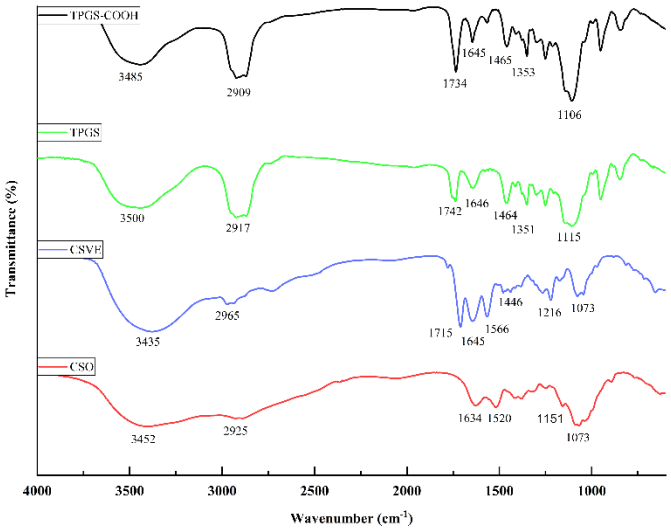

Figure S2. FTIR spectra of TPGS, TPGS-COOH, CSO, and CSVE.

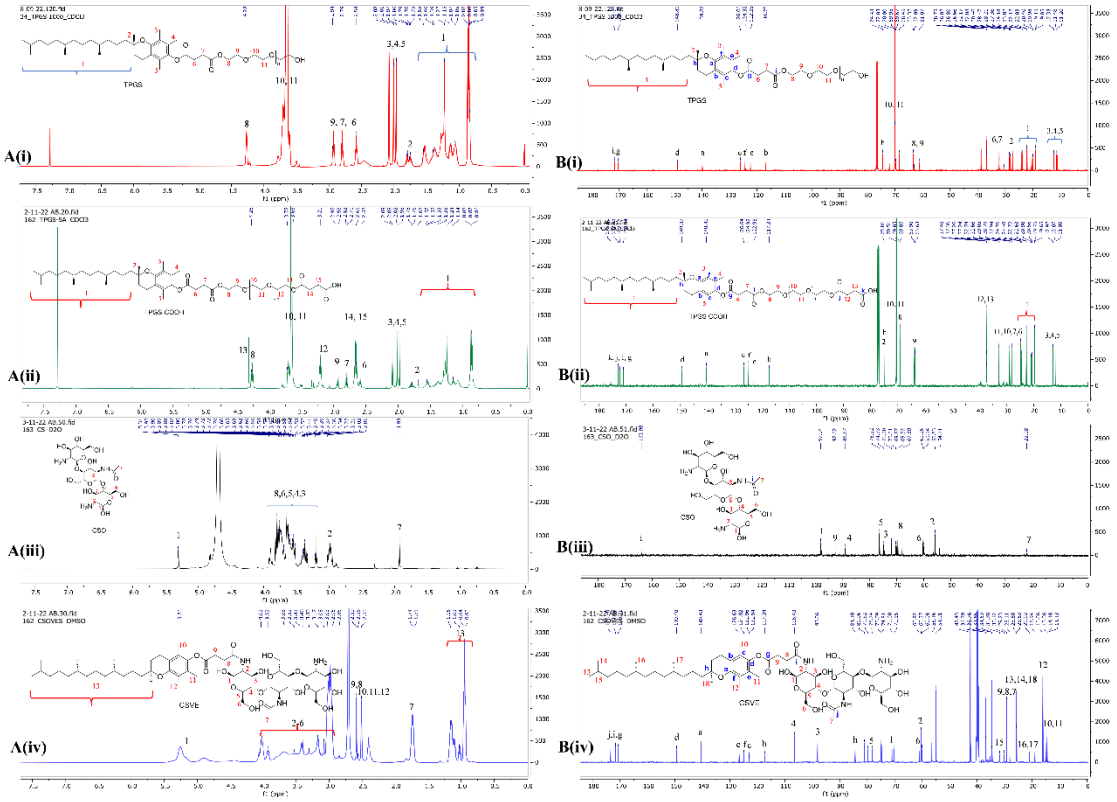

Figure S3. ^{1}H (A) & ^{13}C (B) NMR spectra of (i) TPGS, (ii) TPGS-COOH, (iii) CSO, and (iv) CSVE.

Method 2: Analytical Method Development of Cabazitaxel

The analytical method of cabazitaxel was developed on a High-Performance Liquid

Chromatography (HPLC) instrument (Shimadzu, Japan). The C18 column (150 mm length, 4.6 mm diameter, and 5 µm particle size) was used to develop the analytical method of cabazitaxel. The instrument was attached to a DAD detector and 229 nm was the wavelength used to estimate cabazitaxel concentration. The mobile phase of Acetonitrile (ACN) and 0.3 % acetic acid in water (W0.3aa) at 0.65 and 0.35 volume fractions respectively. The flow rate was maintained at 1 ml min-1. The HPLC chromatogram of Cabazitaxel is provided in Supplementary Information (Figure. S4).

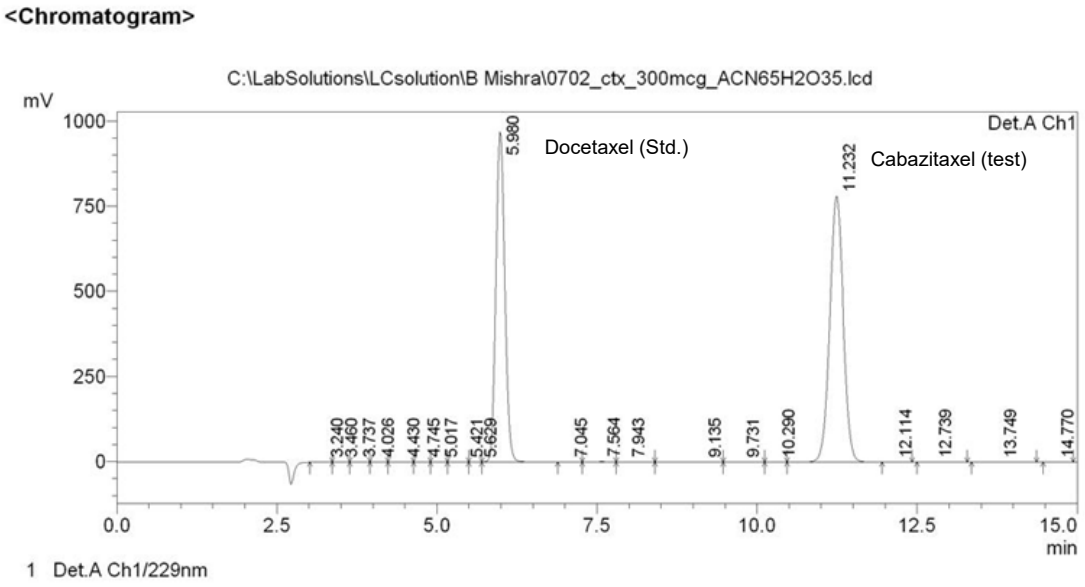

Figure S4. HPLC Chromatogram of Cabazitaxel

Method 3: Bradford assay to determine degree of cetuximab conjugation.

Bradford assay was used to estimate the cetuximab concentration in the purified nanoparticle [5]. A UV-Spectrophotometer-based analytical method was developed to estimate proteins using bovine serum albumin (BSA) as standard. Briefly, various dilutions of BSA were mixed with Bradford's reagent and allowed to rest for 5 minutes. The absorbance was noted at 595 nm wavelength using a UV-Spectrophotometer. The concentration-absorbance curve obtained from the experiment was used to estimate cetuximab conjugated on the surface of the prepared nanoparticles.

Method 4: Solid state characterization

Fourier-transform infrared (FT-IR) spectra of pure drug (CBT), CSVE, HA, TPGS (TPGS-COOH) and all the formulations were acquired using a JASCO FT/IR-4200 type A (JASCO Co., Tokyo, Japan) using KBr method. All spectra were scanned in the range 600–4000 cm−1. Differential scanning calorimetry (DSC) was performed using DSC-60 Plus (Shimadzu, Asia Pacific). 5mg of lyophilized sample was filled in the sealed aluminum pans and analyzed under nitrogen atmosphere at 10 °C/min from 0 to 250 °C. X-ray diffraction (XRD) analysis of lyophilized samples was done using the Rigaku Miniflex 600 Desktop X-Ray Diffraction System (RIGAKU Corporation). Monochromatic CuKα-radiation (λ = 1.5406 Å) was used at 40 mA and at 40 kV over a range of 2θ angles from 0° to 50° with an angular increment of 0.02°/s and scan speed of 1°/min. X-ray photoelectron spectroscopy (XPS) was used to assess the surface chemistry of the formulations. The pellets of lyophilized formulation were used to obtain the spectra on K-Alpha (Thermo Fisher Scientific) with Mg Kα radiation (hν = 1253.6 eV) in the range of 100-700 eV binding energy.

Result 4: Solid state characterization

The FTIR spectra of CBT, CSVE, TPGS, HA, CSVE/HA NP, CSVE/HA/DTPA NP and CSVE/HA/DTPA/Cmab NP were as shown in Fig. 2A. The characteristic peaks of CBT were observed at 3539 cm−1, 3441 cm−1, 3368 cm−1, 3070 cm−1, 2974 cm−1 (a strong peak for N-H stretching of 2˚ amine), 2821 cm−, 2746 cm−1, 1748 cm−1, 1713 cm−1, 1525 cm−1 (C=C Stretching), 1499 cm−1, 1452 cm−1 (-CH3 bending), 1379 cm−1 (-C-N Stretching), 1280 cm−1, 1159 cm−1, 1103 cm−1, 977 cm−1, 949 cm−1, and 714 cm−1 (C-H stretching of benzene). The peaks were similar to previous reports for CBT [6–8]. FTIR spectra of TPGS and CSVE were as discussed above. The FTIR peaks of HA were at 3467 cm−1 corresponding to -OH stretching as broad band, 2927 cm−1 for symmetric methyl -C-H stretch, 1600 cm−1 and 1400 cm−1 were correlated to C-O stretching of COO-, while 1067 cm−1 cm−1 was linked

to C-O-C hemiacetalic system of saccharide units [73,74]. The FTIR spectrum of CSVE/HA nanoparticles exhibited merged peaks of CSVE and HA and similar trend was followed by CSVE/HA/DTPA NP and CSVE/HA/DTPA/Cmab NP. The characteristic peaks of crystalline CBT were masked by CSVE and HA, indicating complete encapsulation of drug in prepared nanoparticles.

The X-Ray diffraction pattern (Fig. 2B) for CBT showed characteristic peaks at 2θ = 7.787˚, 8.873˚, 10.142˚, 12.595˚, 14.326˚, 15.386˚, 17.708˚, 18.573˚, 21.957 ˚, 23.371˚, 26.994˚, and 33.470˚. The XRD spectra of CBT revealed crystalline nature of pure hydrophobic drug and were similar to previously reported peaks [8]. TPGS revealed two peaks of a high intensity at 18.975˚ and 23.323˚ while CSVE had an amorphous halo diffraction pattern with very small intensity peaks. CSVE/HA NP had only two peaks of lower intensity corresponding to TPGS (19.607˚ and 23.742˚). CSVE/HA/DTPA NP exhibited four peaks corresponding to TPGS (19.582˚ and 23.847˚) and DTPA (32.102˚ and 45.838˚). Whereas, reduction in peak intensity in CSVE/HA/DTPA/Cmab NP for DTPA and TPGS may be due to the surface conjugation of Cmab. The crystalline peaks of CBT were absent in all nanoparticles, probably due to peak dominating effect of amorphous polymer CSVE/HA used for nanoparticle preparation.

Thermogram (Fig. 2C) for CBT showed an endothermic peak at 129 ℃. CSVE and HA had no endothermic peak due to amorphous nature. The signature exothermic peak at 228 ℃ was observed for HA. The TPGS exhibited the characteristic endotherm at 40 ℃. While, CSVE/HA NP, CSVE/HA/DTPA, and CSVE/HA/DTPA/Cmab exhibited characteristic peak of TPGS at 36 ℃, 31 ℃, and 30℃, respectively. The slight shifting of TPGS peak can be due to change in particle size.

The XPS spectra of CSO/HA NP and CSVE/HA NP showed signature C1s, N1s, and O1s peaks as shown in Fig. 2D. The atomic percentages of C1s, O1s, and N1s in CSO/HA NP were 68.27%, 25.68% and 6.45% respectively, while CSVE/HA NP yielded atomic percentages of

67.14%, 26.48%, and 6.38% for C1s, O1s, and N1s, respectively. The increase in atomic percentage of O1s may be due to the conjugation of Vitamin E succinate on the CSO backbone. The elemental ratio in CSVE/HA/DTPA NP of 66.11%, 26.82%, and 5.77% for C1s, O1s, and N1s again showed a slight increase in O1s proportion indicating the crosslinking of CSVE by DTPA. This result was further validated due to the presence of 1.3% S2p in the atomic percentages. The proportion of C1s, O1s, N1s, and S2p in CSVE/HA/DTPA/Cmab NP was 64.52%, 23.39%, 9.44%, and 2.65% respectively. A marked increase in N1s and S2p signals indicate the successful conjugation of Cmab on the surface of CSVE/HA/DTPA/Cmab NP. The Cmab is a monoclonal antibody, therefore the amino acids in its sequence results in enhanced signals of N1s and S2p.

Result 5: *In vitro* drug release

The release study was conducted at conditions corresponding to the systemic circulation (pH 7.4), acidic tumor microenvironment (pH 5.5), and intracellular elevated ROS and reduced pH conditions (pH 5.5+GSH). The release profile of CSO/HA NP and CSVE/HA NP exhibited similar trends to CSVE/HA/DTPA NP and CSVE/HA/DTPA/Cmab NP at pH 7.4 and pH 5.5, albeit at higher release rates. However, the release from CSO/HA NP and CSVE/HA NP did not show any marked increase in drug release in the presence of GSH (Fig. S5). The higher release rate in CSVE/HA NP and CSO/HA NP may be attributed to the lack of crosslinking. However, T_{50} for CSVE/HA/DTPA NP at pH 7.4, pH 5.5 and pH 5.5+GSH were 18h, 7.5h, and 2.5 h. respectively. The difference in the extent of drug release from the redox responsive system in comparison to CSO/HA NP and CSVE/HA NP in the presence of GSH was significantly higher. The release rate was highest in pH 5.5 + GSH (10mM) followed by pH 5.5 and pH 7.4. The acidic pH and GSH induces faster drug release from formulated nanoparticles, while exhibiting slow and sustained drug release at physiological pH (pH 7.4). Also, T_{50} for CSVE/HA/DTPA/Cmab NP at pH 7.4, pH 5.5 and pH 5.5+GSH were 15h, 8.5h,

and 2.5 h, respectively, exhibiting a similar trend to CSVE/HA/DTPA NP. In other words, CSVE/HA/DTPA/Cmab NP in pH 7.4, pH 5.5 and pH 5.5+GSH showed drug release of about 8%, 10%, and 24% in 1h and 45%, 60%, and 98% in 12h (Fig. 3A). The pH-responsive trend in the release behavior of all the particles can be attributed to protonation of the amino groups on CS at lower pH value responsible for enhanced electrostatic repulsion and thus easy diffusion of loaded drug from NPs [1,9]. However, the increased release of drug in the media comprising low pH and GSH is due to the cleavage of disulfide bonds of the crosslinker DTPA in response to GSH ([10–12]. The GSH-responsive cleavage of disulfide linkage was further confirmed by Ellman's reagent that showed a rapid release of free thiol group in CSVE/HA/DTPA NP in first 90 min when exposed to Acetate buffer (pH 5.5) + GSH, described below (Method 6 and Result 6). The limited and slow release of drug from nanoparticles at pH 7.4 would be beneficial as it will prevent off-site release of the drug in systemic circulation and majority of drug will be released only in tumor microenvironment.

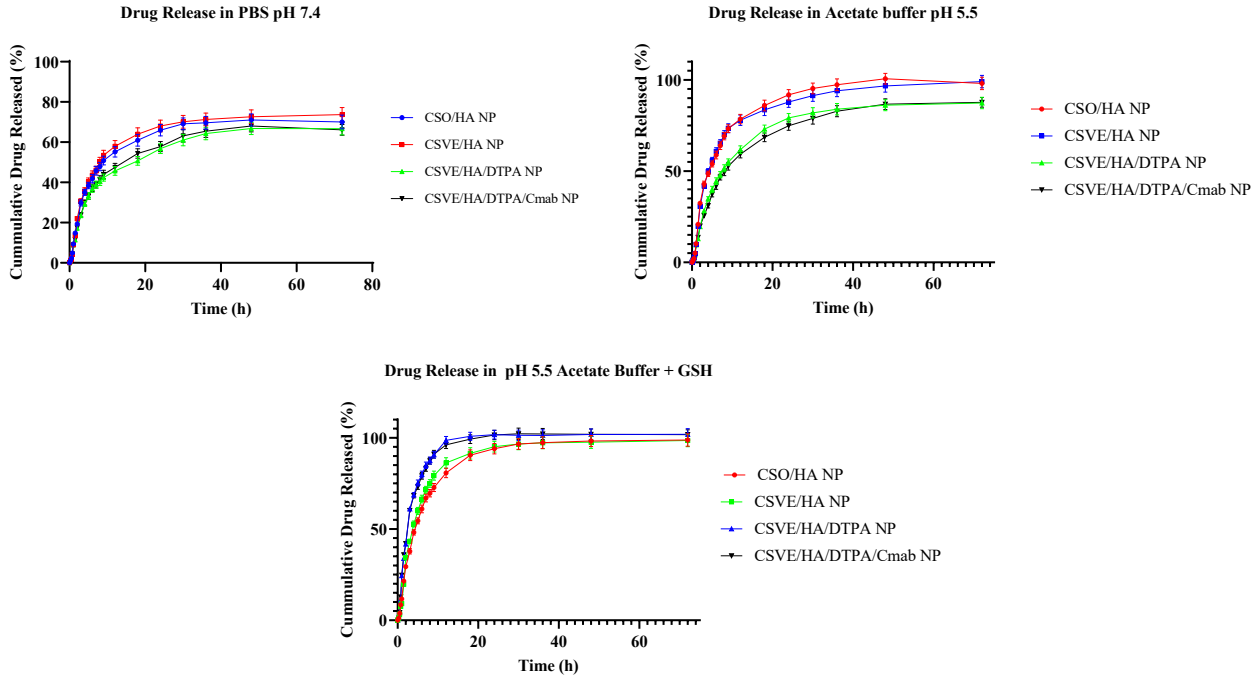

Figure S5. In-vitro drug release of CSO/HA NP, CSVE/HA NP, CSVE/HA/DTPA NP, and CSVE/HA/DTAPA/Cmab NP in pH 7.4, pH 5.5, and pH 5.5+GSH.

Supplementary Table 1: R-square values for mathematical models employed to determine the goodness of fit.

	CSVE/HA/ DTPA NP (pH 7.4)	CSVE/HA/DTPA/Cmab NP (pH 7.4)	CSVE/HA/ DTPA NP (pH 5.5)	CSVE/HA/DTPA/Cmab NP (pH 5.5)	CSVE/HA/ DTPA NP (pH 5.5 + GSH)	CSVE/HA/DTPA/Cmab NP (pH 5.5 + GSH)
Hixson-Crowell	0.6139	0.6267	0.8913	0.8988	0.4209	0.4285
Hopfenberg	0.7248	0.7356	0.9591	0.9556	0.9933	0.9933
Baker-Lonsdale	0.9331	0.9271	0.9557	0.9634	0.5597	0.5715
Makoid-banakar	0.9799	0.9827	0.9866	0.9885	0.9405	0.9453
Quadratic	0.7592	0.7663	0.8154	0.8352	0.3343	0.3438
Weibull	**0.9885 β= 0.419**	**0.9860 β= 0.421**	0.9944	0.9967	**0.9979 β= 0.850**	**0.9982 β= 0.805**
Logistic	0.9947	0.9941	**0.9985 β= 2.773**	**0.9986 β= 2.588**	**0.9973 β= 3.521**	**0.9972 β= 3.364**
Gompertz	**0.9950 β= 1.051**	**0.9962 β= 1.082**	0.9959	0.9950	0.9901	0.9901
Probit	0.9834	0.9813	**0.9971 β= 1.490**	**0.9985 β= 1.450**	0.9968	0.9967
Higuchi	0.8626	0.8507	0.8729	0.8996	0.5148	0.5244
First Order	0.7249	0.7358	0.9591	0.9556	0.9930	0.9934
Zero order	0.1487	0.1248	0.2259	0.2956	-0.6505	-0.6481
Peppas and Sahlin	0.9792	0.9810	0.9831	0.9864	0.9329	0.9389
Korsmeyer Peppas	0.9816	0.9836	0.9865	0.9715	0.9749	0.9690

Method 6. Ellman's assay for in-solution quantification of sulfhydryl groups

Ellman's reagent is 5,5'-dithio-bis-(2-nitrobenzoic acid), also known as DTNB, a compound used for quantitating free sulfhydryl groups in solution. DTNB produces a yellow-colored product on reacting with sulfhydryl groups, that can be quantified by measuring absorbance at 412 nm using a spectrophotometer.

Ellman's Reagent was used to determine the redox responsive behavior of CSVE/HA/DTPA NP. Firstly, Ellmans reagent (80µg/ml) in buffer solutions (0.1 M sodium phosphate, pH 8.0, containing 1 mM EDTA) was prepared. Then, 300mg of CSVE/HA/DTPA NP weigh was incubated in 20 ml of acetate buffer (pH 5.5) with GSH (150 mg; ~0.5 millimole). 250µl of aliquots were collected at 5, 15, 30, 45, 60, 90, and 120min and samples were incubated with

2.5ml of Ellman's Reagent Solution for 15 min. 200 µl incubated solution was transferred in 96 well plate and absorbance were measured at 412nm using microplate reader. The absorbance vs time graph was plotted.

Results 6. In the presence of GSH, the disulfide linkage of the crosslinker (DTPA) is cleaved to release free thiol groups that will bind to Ellman's Reagent to give yellow color. The absorbance intensity at 412nm is a direct indicative of the amount of free thiol group. The graph below shows time dependent increase in free thiol groups in CSVE/HA/DTPA incubated in GSH enriched media for 60 min and then becomes constant (**Figure S6**).

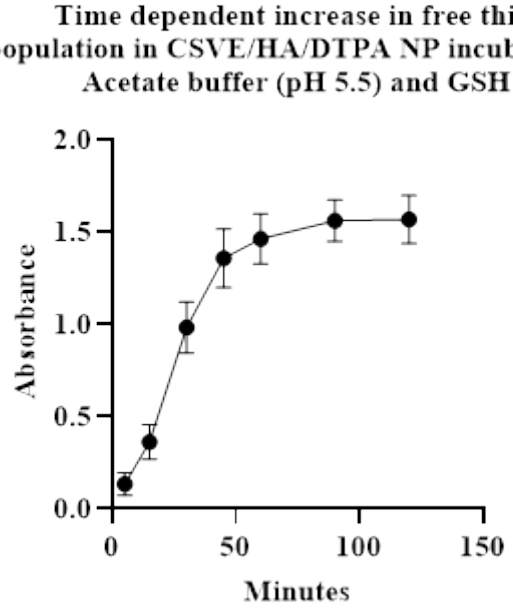

Figure S6.

Method 7. Stability of nanoparticles

To determine the stability of the nanoparticles prepared, the lyophilized nanoparticles were stored in air tight borosilicate glass vials at 4 °C for predetermined intervals. After day 7, 15, 30, 90, and 180, the lyophilized nanoparticles were resuspended in deionized water and checked for change in hydrodynamic diameter, zeta potential, PDI, and entrapment efficiency using methods detailed in the manuscript (see methods in main manuscript).

Result 7: The hydrodynamic size, zeta potential, PDI, and entrapment efficiency of CSVE/HA/DTPA NP and CSVE/HA/DTPA/Cmab did not show any significant (p value > 0.9) change even after storage for 180 days (**Figure S7**). The non-significant change in these characteristics may be attributed to the hydrophilic surface of the nanoparticles due to the presence of pegylated chain on the surface of nanoparticles, hyaluronic acid (a hydrophilic polysaccharide), and cetuximab (in case of CSVE/HA/DTPA/Cmab NP). The hydrophilic environment around the nanoparticle corona ensures optimal hydration on nanoparticles while resuspension resulting in the formation of monodispersed nanosuspension. In case of entrapment efficiency, this insignificant change indicate that the nanoparticles do not show any drug leaking from the nanocarrier due to lyophilization and storage, suggesting the formation of a stable carrier system for lipophilic drugs like cabazitaxel.

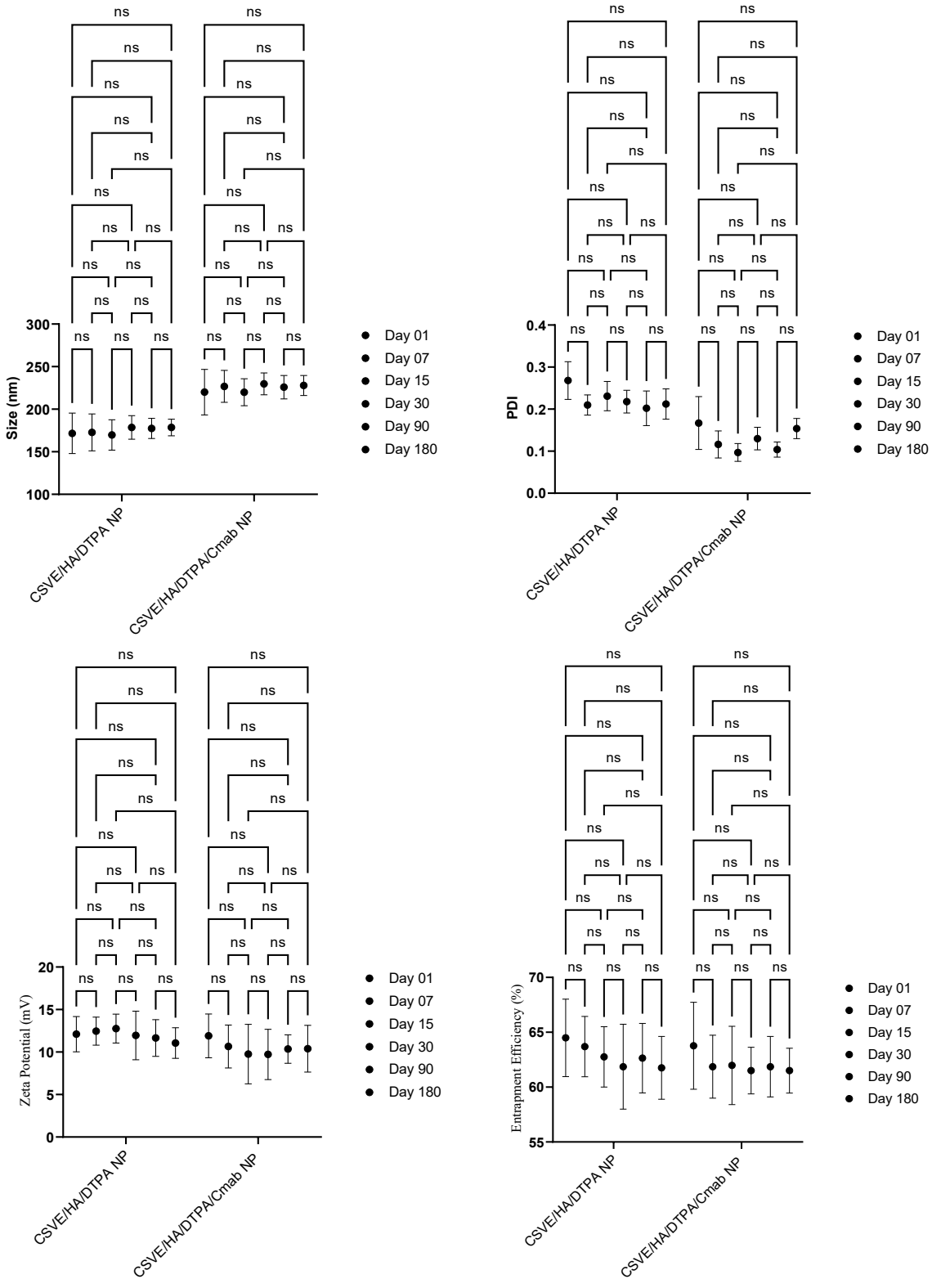

Figure S7: Effect of storage of lyophilized nanoparticles on Particle size (hydrodynamic diameter), PDI, zeta potential, and entrapment efficiency.

Method 8. Cell Viability Assay

The cytotoxicity of the prepared formulations were examined by MTT (3-(4, 5-dimethylthiazolyl-2)-2, 5-diphenyltetrazolium bromide) assay [13]. MDA-MB-231, T47D, and HCT116 cells were grown in an incubator at 37 °C under 5% CO_2 condition with their respective media. After the cells were harvested, they were counted and seeded at 1×10^5 cells per well in a 96-well plate overnight. The following day, cells were exposed to various concentrations of Blank Formulation, Standard (Cabazitaxel), cabazitaxel loaded hybrid CSO-HA nanoparticle (CSO/HA NP), cabazitaxel loaded hybrid CSVE-HA nanoparticle (CSVE/HA NP), cabazitaxel loaded redox responsive hybrid CSVE-HA nanoparticle (CSVE/HA/DTPA NP) and Cetuximab conjugated cabazitaxel loaded redox responsive hybrid CSVE-HA nanoparticle (CSVE/HA/DTPA/Cmab). Then, the treated cells were incubated for 24 h. Following incubation, 100 µL of (5 mg/mL) MTT reagent dissolved in media was added to each well and then cells were incubated for another two hours. Subsequently, the solution was removed and 100 µL of dimethyl sulfoxide (DMSO) was added to the wells. Afterward, the plate was read at 570 nm using a microplate reader. The following formula was used to determine the percentage of viable cells:

$$Percentage\ of\ viability\ (\%) = \frac{(Absorbance\ of\ sample\ at\ 570\ nm)}{(Absorbance\ of\ control\ at\ 570\ nm)} \times\ 100$$

Result 8. Cell Viability Assay

To investigate the cytotoxicity and antiproliferative activity of the formulations, MDA-MB-231, T47D, and HCT116 cells were exposed to various concentrations for 24 h and their IC_{50} values were determined. The formulations; CSO/HA NP, CSVE/HA NP, CSVE/HA/DTPA NP, and CSVE/HA/DTPA/Cmab NP induced significant concentration-dependent inhibition on the MDA-MB-231 cell line (Fig. 3B). MTT data revealed that formulations exhibit a substantial suppressive effect on the proliferation of the MDA-MB-231 cell line. The CSO/HA NP showed an IC_{50} value of 2.816 ± 0.182 µg/ml, which was a 1.25-fold reduction compared

to cabazitaxel (3.521 ± 0.294 µg/ml). Also, the IC_{50} value of non-targeted redox responsive CSVE/HA/DTPA NP and CSVE/HA NP was found to be 2.105 ± 0.133 µg/ml and 2.358 ± 0.167 µg/ml, respectively. However, CSVE/HA/DTPA/Cmab NP elicited the highest inhibitory effect, showing IC_{50} value at 1.04 ± 0.185 µg/ml concentration in MDA-MB-231 cells. This could be attributed to increased internalization of CSVE/HA/DTPA/Cmab NP via receptor-mediated endocytosis. To confirm this, cellular uptake study was conducted in MDA-MB-231 cells.

When HCT116 cells were treated with various concentrations of the prepared formulations for 24 hours, a concentration dependent decline in cell viability was observed with all the Cabazitaxel loaded formulation and Cabazitaxel. The observed IC_{50} for Cabazitaxel, CSO/HA NP, CSVE/HA NP, CSVE/HA/DTPA NP, and CSVE/HA/DTPA/Cmab NP was found to be 5.924 ± 0.724 µg/ml, 3.490 ± 0.283 µg/ml, 2.167 ± 0.171 µg/ml, 2.205 ± 0.102 µg/ml, 2.158 ± 0.159 µg/ml respectively (normalized cell viability versus time graph in Figure 3). The results show a significant decline in IC_{50} of CSVE based nanoparticles, but surface conjugation with Cetuximab did not yield any significant reduction in IC_{50}.

Similar observations were made when the T47D cells were treated with the prepared nanoparticles. The groups exposed to varying concentrations of Cabazitaxel, CSO/HA NP, CSVE/HA NP, CSVE/HA/DTPA NP, and CSVE/HA/DTPA/Cmab NP the IC_{50} was found to be 6.675 ± 0.502 µg/ml, 5.651 ± 0.318 µg/ml, 3.043 ± 0.186 µg/ml, 3.195 ± 0.295 µg/ml, and 2.849 ± 0.143 µg/ml, respectively (normalized cell viability versus time graph in Figure 3). The non-significant difference in the IC_{50} value of CSVE/HA/DTPA NP and CSVE/HA/DTPA/Cmab NP treated groups may be attributed to lower expression of EGFR on the surface of these cell line which is highly expressed on MDA-MB-231 indicating the possible selectivity of CSVE/HA/DTPA/Cmab NP towards the cells over expressing EGFR.

This observation was further confirmed by assessing the effect of EGFR-blocking on the cellular uptake of CSVE/HA/DTPA/Cmab NP in MDA-MB-231 cells.

References

[1] Y. Guo, M. Chu, S. Tan, S. Zhao, H. Liu, B.O. Otieno, X. Yang, C. Xu, Z. Zhang, Chitosan-g-TPGS Nanoparticles for Anticancer Drug Delivery and Overcoming Multidrug Resistance, Mol. Pharm. 11 (2014) 59–70. https://doi.org/10.1021/mp400514t.

[2] Y. Chen, S. Feng, W. Liu, Z. Yuan, P. Yin, F. Gao, Vitamin E Succinate-Grafted-Chitosan Oligosaccharide/RGD-Conjugated TPGS Mixed Micelles Loaded with Paclitaxel for U87MG Tumor Therapy, Mol. Pharm. 14 (2017) 1190–1203. https://doi.org/10.1021/acs.molpharmaceut.6b01068.

[3] A.M. Itoo, M. Paul, B. Ghosh, S. Biswas, Oxaliplatin delivery via chitosan/vitamin E conjugate micelles for improved efficacy and MDR-reversal in breast cancer, Carbohydr. Polym. 282 (2022) 119108. https://doi.org/10.1016/j.carbpol.2022.119108.

[4] B. Wei, M. He, X. Cai, X. Hou, Y. Wang, J. Chen, M. Lan, Y. Chen, K. Lou, F. Gao, Vitamin E succinate-grafted-chitosan/chitosan oligosaccharide mixed micelles loaded with C-DMSA for Hg2+ detection and detoxification in rat liver, Int. J. Nanomedicine 14 (2019) 6917. https://doi.org/10.2147/IJN.S213084.

[5] A. Cimini, B. D'Angelo, S. Das, R. Gentile, E. Benedetti, V. Singh, A.M. Monaco, S. Santucci, S. Seal, Antibody-conjugated PEGylated cerium oxide nanoparticles for specific targeting of Aβ aggregates modulate neuronal survival pathways, Acta Biomater. 8 (2012) 2056–2067. https://www.sciencedirect.com/science/article/pii/S1742706112000517 (accessed November 28, 2023).

[6] P. Chand, H. Kumar, N. Badduri, N.V. Gupta, V.G. Bettada, S.V. Madhunapantula, S.S. Kesharwani, S. Dey, V. Jain, Design and evaluation of cabazitaxel loaded NLCs against breast cancer cell lines, Colloids Surf. B Biointerfaces 199 (2021) 111535. https://doi.org/10.1016/j.colsurfb.2020.111535.

[7] W. Cabri, D. Ciceri, L. Domenighini, A. Gambini, F. Peterlongo, A crystalline anhydrous form of cabazitaxel, process for the preparation and pharmaceutical compositions thereof, EP3060556A1, 2016. https://patents.google.com/patent/EP3060556A1/en (accessed November 26, 2023).

[8] A.K. Jangid, D. Pooja, P. Jain, S.V.K. Rompicharla, S. Ramesan, H. Kulhari, A nanoscale, biocompatible and amphiphilic prodrug of cabazitaxel with improved anticancer efficacy against 3D spheroids of prostate cancer cells, Mater. Adv. 1 (2020) 738–748. https://doi.org/10.1039/D0MA00189A.

[9] Q. Chen, C. Jia, Y. Xu, Z. Jiang, T. Hu, C. Li, X. Cheng, Dual-pH responsive chitosan nanoparticles for improving in vivo drugs delivery and chemoresistance in breast cancer, Carbohydr. Polym. 290 (2022) 119518. https://doi.org/10.1016/j.carbpol.2022.119518.

[10] A. Sood, A. Gupta, R. Bharadwaj, P. Ranganath, N. Silverman, G. Agrawal, Biodegradable disulfide crosslinked chitosan/stearic acid nanoparticles for dual drug delivery for colorectal cancer, Carbohydr. Polym. 294 (2022) 119833. https://doi.org/10.1016/j.carbpol.2022.119833.

[11] F. Wang, J. Li, C. Chen, H. Qi, K. Huang, S. Hu, Preparation and synergistic chemo-photothermal therapy of redox-responsive carboxymethyl cellulose/chitosan complex nanoparticles, Carbohydr. Polym. 275 (2022) 118714. https://doi.org/10.1016/j.carbpol.2021.118714.

[12] H. Vakilzadeh, J. Varshosaz, M. Dinari, M. Mirian, V. Hajhashemi, N. Shamaeizadeh, H.M. Sadeghi, Smart redox-sensitive micelles based on chitosan for dasatinib delivery in suppressing inflammatory diseases, Int. J. Biol. Macromol. 229 (2023) 696–712. https://doi.org/10.1016/j.ijbiomac.2022.12.111.

[13] F. Chen, J. Zhang, L. Wang, Y. Wang, M. Chen, Tumor pHe-triggered charge-reversal and redox-responsive nanoparticles for docetaxel delivery in hepatocellular carcinoma treatment, Nanoscale 7 (2015) 15763–15779. https://doi.org/10.1039/C5NR04612B.